Functionalized mesoporous silicas SBA-15 for heterogeneous photocatalysis towards CECs removal from secondary urban wastewater

Bruna Castanheira[a], Larissa Otubo[b], Cristiano L. P. Oliveira[c], Rosa Montes[d], José Benito Quintana[d], Rosario Rodil[d], Sergio Brochsztain[e], Vítor J. P. Vilar[f], Antonio Carlos S. C. Teixeira[a,*]

[a]Research Group in Advanced Oxidation Processes (AdOx), Chemical Systems Engineering Center, Department of Chemical Engineering, University of São Paulo, Av. Prof. Luciano Gualberto, tr. 3, 380, São Paulo, SP, Brazil

[b]Nuclear and Energy Research Institute (IPEN), Av. Prof. Lineu Prestes, 2242, 05508-000, São Paulo, SP, Brazil. [c]Institute of Physics, University of São Paulo, Rua do Matão 1371, 05508-090, São Paulo, SP, Brazil

[d]Department of Analytical Chemistry, Nutrition and Food Sciences, Institute of Research on Chemical and Biological Analysis (IAQBUS), Universidade de Santiago de Compostela, Constantino Candeira S/N, 15782 Santiago de Compostela, Spain.

[e]Federal University of ABC, Av. dos Estados, 5001, 09210-580, Santo André, SP, Brazil.

[f]Laboratory of Separation and Reaction Engineering-Laboratory of Catalysis and Materials (LSRE-LCM), Department of Chemical Engineering, Faculty of Engineering, University of Porto, Rua Dr. Roberto Frias, 4200-465 Porto, Portugal.

Corresponding author: Antonio Carlos S. C. Teixeira (acscteix@usp.br).

Highlights

- First study using TiO_2/SBA-15 for CECs oxidation in an annular FluHelik photoreactor.
- Removal of sulfadiazine (SDZ) from pure water and urban waste water (UWW) spiked with SDZ.
- The activity of TiO_2/SBA-15 in UWW was higher than that of standard TiO_2-P25 for SDZ degradation.
- Adsorption and/or photocatalysis were able to remove other 65 CECs detected in the UWW matrix.

Functionalized mesoporous silicas SBA-15 for heterogeneous photocatalysis towards CECs removal from secondary urban wastewater

Bruna Castanheira[a], Larissa Otubo[b], Cristiano L. P. Oliveira[c], Rosa Montes[d], José Benito Quintana[d], Rosario Rodil[d], Sergio Brochsztain[e], Vítor J. P. Vilar[f], Antonio Carlos S. C. Teixeira[a,*]

[a]Research Group in Advanced Oxidation Processes (AdOx), Chemical Systems Engineering Center, Department of Chemical Engineering, Escola Politécnica, University of São Paulo, Av. Prof. Luciano Gualberto, tr. 3, 380, São Paulo, SP, Brazil

[b]Nuclear and Energy Research Institute (IPEN), Av. Prof. Lineu Prestes, 2242, 05508-000, São Paulo, SP, Brazil. [c]Institute of Physics, University of São Paulo, Rua do Matão 1371, 05508-090, São Paulo, SP, Brazil

[d]Department of Analytical Chemistry, Nutrition and Food Sciences, Institute of Research on Chemical and Biological Analysis (IAQBUS), Universidade de Santiago de Compostela, Constantino Candeira S/N, 15782 Santiago de Compostela, Spain.

[e]Federal University of ABC, Av. dos Estados, 5001, 09210-580, Santo André, SP, Brazil.

[f]Laboratory of Separation and Reaction Engineering-Laboratory of Catalysis and Materials (LSRE-LCM), Department of Chemical Engineering, Faculty of Engineering, University of Porto, Rua Dr. Roberto Frias, 4200-465 Porto, Portugal.

Corresponding author: Antonio Carlos S. C. Teixeira (acscteix@usp.br).

Abstract

The photocatalytic activity of TiO_2 nanoparticles (NP) supported on mesoporous silica SBA-15 (TiO_2/SBA-15) was evaluated for the photodegradation of sulfadiazine (SDZ), as target contaminant of emerging concern (CEC), using either pure water solutions (PW) or a real secondary urban wastewater (UWW) spiked with SDZ. For this purpose, TiO_2/SBA-15 samples with 10, 20 and 30% TiO_2 (w/w) were prepared by the sol-gel post synthetic method on pre-formed SBA-15, using titanium (IV) isopropoxide as a precursor. The TiO_2/SBA-15 materials were characterized by HRTEM, SAXS and XRD, nitrogen adsorption isotherms and UV-vis diffuse reflectance spectroscopy. TiO_2 NPs were shown to be attached onto the external surface, decorating the SBA-15 particles. The TiO_2/SBA-15 catalysts were active in SDZ photodegradation using the annular FluHelik photoreactor, when irradiated with UVA light. The 30% TiO_2/SBA-15 sample presented the best performance in optimization tests performed using PW, and it was further used for the tests with UWW. The photocatalytic activity of 30% TiO_2/SBA-15 was higher (56% SDZ degradation) than that of standard TiO_2-P25 (32% SDZ degradation) in the removal of SDZ spiked in the UWW ([SDZ] = 2 mg L^{-1}). The photodegradation of SDZ with 30% TiO_2/SBA-15 reached 90% when a UWW spiked with a lower SDZ concentration ([SDZ] = 40 µg L^{-1}). Aside of SDZ, a suit of 65 other CECs were also identified in the UWW sample using LC-MS spectrometry. A fast-screening test showed the heterogeneous photocatalytic system was able to remove most of the detected CECs from UWW, by either adsorption and/or photocatalysis.

Keywords: Advanced Oxidation Processes; Photocatalysis; Mesoporous Silicas; FluHelik Photoreactor; Sulfadiazine.

1. Introduction

The shortage of good quality water supplies for the world population has become one of the main challenges of the 21st century. In addition to the pollutants commonly found in water, a new class of contaminants has gained increasing attention in recent years. The so-called contaminants of emerging concern (CECs) are synthetic or natural substances found at low concentrations (ng L^{-1} to µg L^{-1}) in water bodies, and which are suspect of causing hazardous effects to the ecosystem and to the human health (Krzeminski et al., 2019; Rivera-Utrilla et al., 2013; Rodriguez-Narvaez et al., 2017). Pharmaceutical products, antibiotics, hormones and pesticides are relevant examples of CECs. CECs are not regularly monitored in the environment, as there is no regulation for their control in most countries. They are usually not eliminated by conventional water treatment methods, and are then disposed into the environment, where they may accumulate in living organisms. Moreover, wastewater reuse for agriculture might lead to the introduction of CECs in the food chain. Urban wastewaters treatment plants (WWTPs) are the main sources of CECs released into the environment, which can induce bacterial resistance and cause damage to aquatic ecosystems (Kovalakova et al., 2020; Kümmerer, 2009a, 2009b).

Different methods for advanced wastewater treatment have been considered in attempt to remove CECs from WWTPs, including adsorption, membrane filtration, ozonation and advanced oxidation processes (AOPs) (Krzeminski et al., 2019; Mohammad et al., 2017; Rivera-Utrilla et al., 2013; Rodriguez-Narvaez et al., 2017). Among AOPs, TiO_2-based photocatalysis has been acknowledged as a promising alternative for CECs removal (Fagan et al., 2016; Miranda-García et al., 2014, 2010). TiO_2 NPs are low-cost, nontoxic, chemically and physically stable. However, commercially available TiO_2 (e.g. P-25) poses some drawbacks, such as low surface area and a tendency to agglomerate in aqueous media. Moreover, small TiO_2 particles are difficult to recover by filtration or centrifugation, leading to a difficult separation and recycle, thus limiting its application in industrial scale (Dong et

al., 2015). To avoid those problems, in this work it was adopted a strategy reported by several authors, namely the immobilization of TiO_2 onto mesoporous silica SBA-15 (Acosta-Silva et al., 2011; Araújo et al., 2016; Besançon et al., 2016; Busuioc et al., 2006; Calzada et al., 2019; Conceição et al., 2017; Lachheb et al., 2011; Liou et al., 2018; Liu et al., 2016; López-Muñoz et al., 2005; Mehta et al., 2016; Salameh et al., 2015; Tseng et al., 2012; Van Grieken et al., 2002; Wei et al., 2018; Yang et al., 2006; Yuan et al., 2020). Different techniques have been employed for the functionalization of SBA-15 with TiO_2, including incipient wet impregnation (Calzada et al., 2019), microwave assisted technique (Mehta et al., 2016), direct synthesis (Liou et al., 2018) and sol-gel post-synthetic method, (Conceição et al., 2017; Yang et al., 2006) which was the technique employed in the present work. In general, TiO_2/SBA-15 materials have shown good efficiency for the degradation of CECs such as dyes (Acosta-Silva et al., 2011; Calzada et al., 2019; Tseng et al., 2012) and other industrial organic contaminants (Conceição et al., 2017; Mehta et al., 2016; Yuan et al., 2020).

To our knowledge, however, all those investigations were limited to batch reactors and synthetic solutions of the contaminant, which are hard to scale up to real systems. In this context, a new concept of light-driven scalable reactor, the annular FluHelik reactor (Espíndola et al., 2019; Moreira et al., 2019) (Figure S1), which consists of a cylindrical stainless steel shell with inlet and outlet pipes located perpendicularly to the fluid flow on opposite sites and tangentially to the reactor tube in horizontal plane. The single and cylindrical UV lamp is located in a concentric inner quartz sleeve. This design leads to a helicoidal flow around the quartz sleeve allowing a more intense macromixing dynamics, as well as homogenous UV fluence (Figure S1). Furthermore, the design of the FluHelik photoreactor favors the implementation of several reactors in series, promoting their application on an industrial scale (Espíndola and Vilar, 2020). The FluHelik photoreactor has been successfully employed for homogenous photochemical reactions, such as

UVC/H_2O_2, UVC/O_3 and photo-Fenton, targeting the treatment of leachates from sanitary landfills (pre-industrial scale) (Gomes, et al., 2018), slaughterhouse wastewater and CECs removal from secondary urban wastewaters (Alfonso-Muniozguren et al., 2021; Gomes, et al., 2021; Barbosa et al., 2020; Espíndola et al., 2019; Espíndola et al.,2021). However, the FluHelik reactor has not yet been tested for AOPs involving heterogeneous catalysis.

In the present work, the FluHelik reactor was used to promote heterogeneous photocatalysis, using a functionalized silica consisting of TiO_2 nanoparticles (NPs) supported on SBA-15 mesoporous silica. The system was tested for the photodegradation of sulfadiazine (SDZ) selected as a model of CEC. An example of sulfonamide antibiotics, SDZ is predominantly eliminated in its original form; due to its high stability, about 30-90% of the ingested dose is not absorbed by the body. As a weak acid, SDZ has high solubility (77 mg L^{-1}) and water mobility and has been found in water bodies and wastewater (Balakrishnan et al., 2006; García-Galán et al., 2011). In addition to being able to induce bacterial resistance, SDZ can also cause toxic effects and act as an endocrine disruptor in several living organisms and possibly in humans (Baran et al., 2011; Paulus et al., 2019).

The photocatalytic efficiency of TiO_2/SBA-15 in the FluHelik photoreactor was optimized for SDZ oxidation using pure water solutions. Furthermore, the TiO_2/SBA-15 photocatalysts were also active in the degradation of SDZ spiked in real urban waste water (UWW), collected after secondary treatment and tested as a real matrix.

Recently, new analytical methods employing high-resolution mass spectrometry combined with liquid chromatography-quadrupole-time of flight mass spectrometer (LC-QTOF) have allowed the screening of a large number of CECs in water bodies at the ng L^{-1} to μg L^{-1} level in a single run (Paíga et al., 2019; Schymanski et al., 2014; Castro et al., 2021; Wilson et al., 2021). Using LC-QTOF, we were able to detect 65 other CECs present in the UWW sample. Remarkably, irradiation of the UWW in the FluHelik reactor with the TiO_2/SBA-15

126 photocatalysts led to a reduction in the concentration of most of these CECs initially present
127 in the UWW.

128 **2. Experimental**

129 *2.1 Chemicals*

130 The following reagents were obtained from Sigma-Aldrich: Pluronic P123 (amphiphilic
131 triblock copolymer, average molecular weight 5,800, 97% purity), tetraethyl orthosilicate
132 (TEOS), sulfadiazine (SDZ, 99% purity) and titanium (IV) isopropoxide (TTIP, 97% purity).
133 Hydrochloric acid and isopropanol were purchased from Baker. Standard TiO_2 (Aeroxide®
134 P-25; purity ≥ 99.5%; specific surface area 55 m^2 g^{-1}) was obtained from Evonik. The real
135 wastewater sample was collected after the secondary treatment of an urban wastewater
136 (UWW) from Portugal in October 2019. Its physicochemical characteristics are summarized
137 in Table S1.

138 *2.2 Catalysts synthesis*

139 *2.2.1 Synthesis of pristine SBA-15*

140 The pure SBA-15 matrix was synthesized according to the standard procedure (Zhao et al.,
141 1998), as follows: 4.1 g of Pluronic P123 was dissolved in 30 mL of deionized water under
142 stirring at 35 °C, then 120 g of 2 M HCl aqueous solution was added, and the mixture was
143 stirred for 2 h. In the sequence, 8.5 g (41 mmol) of tetraethylorthosilicate (TEOS) was added
144 and the system was maintained at 35 °C for 24 h under constant stirring. Thereafter, the
145 formed gel was transferred to a mini autoclave, which was sealed and subjected to
146 hydrothermal conditions at 100 °C for 24 h. The sample obtained was washed with 2 L of
147 deionized water, and the precipitated solid was filtrated under vacuum, washed once again
148 with 1 L of deionized water and dried under vacuum for 48 h. Finally, the resulting material
149 was subjected to calcination at 500 °C under N_2 atmosphere for 4 h with a heating rate of 10
150 °C min^{-1} to decompose the triblock copolymer and obtain the SBA-15.

151

152 *2.2.2 Functionalization of SBA-15 with titanium dioxide*

153 The titanium dioxide crystals were deposited onto the SBA-15 surface via sol-gel processing
154 according to the procedure described by Yang et al. (Yang et al., 2006) For this purpose,
155 SBA-15 (1.0 g) was sonicated in 50 mL of isopropanol. Different amounts of TTIP were
156 then added, in order to produce samples with different TiO_2 contents, as given in Table 1.
157 Deionized water was slowly added to the resulting mixture (TTIP/water with volumetric
158 ratio of 1/10) to guarantee the hydrolysis of the TTIP. The mixture was stirred for 2 h at
159 room temperature, followed by centrifugation and washing with deionized water. The solid
160 product was dried at 80 °C overnight and then calcined in air at 700 °C for 2 h to obtain the
161 *x%*TiO_2/SBA-15 catalysts, where *x%* represents the wt% of titania loading (Table 1).

162

163 **Table 1.** Description of the TiO_2/SBA-15 samples prepared.

Sample	Volume TTIP (mL)[a]	Weight % TiO_2	Ti/Si[b]
10% TiO_2/SBA-15	0.37	10%	0.08
20% TiO_2/SBA-15	0.74	20%	0.15
30% TiO_2/SBA-15	1.11	30%	0.23

164 [a] Added to 1 g of SBA-15 (d_{TTIP} = 0.96 g cm^{-3}). [b] Molar ratio.

165

166 *2.3 Catalysts characterization*

167 The pristine SBA-15 and TiO_2/SBA-15 materials were structurally characterized by N_2
168 physisorption at 77 K using the Nova 2200 Surface Area and Pore Size Analyzer
169 (Quantachrome). The surface areas were obtained by the BET method, pore volumes were
170 calculated at P/P_0 = 0.97 and average pore diameters were obtained by the BJH method
171 (desorption branch).

High resolution transmission electron microscopy (HRTEM) images were obtained with a JEOL JEM 2100 microscope operating at 200 kV. Samples for HRTEM were prepared by drop-casting on aqueous suspension of the mesoporous materials over a carbon-coated copper grid, followed by drying under room conditions. Average particle sizes were calculated from the TEM images with the aid of ImageJ software, by averaging over a large number of individual particles (typically 50-250 NPs).

Small angle X-ray scattering measurements (SAXS) were carried out using a Xeuss 2.0 equipment, with a generating source Xenocs with CuKα (λ = 0.15406 nm) radiation. All the samples were scanned under the same conditions in the range 2θ = 0-3°. The hexagonal cell parameter (a_0) was determined according to Equation 1, where d_{100} corresponds to the Bragg's distance reflection at the (100) crystallography plane.

$$a_0 = \frac{2d_{100}}{\sqrt{3}} \quad (1)$$

The TiO_2 nanocrystals present on the TiO_2/SBA-15 materials were characterized with wide-angle XRD patterns recorded on a Bruker (D8-Discover) powder X-ray diffractometer using CuKα, radiation of wavelength 0.15406 nm (40 KV, 30 mA), LynxEye detector and Ni filter in the 2θ range 10°-100° with a scanning velocity of 0.75° min^{-1}. From the line broadening of the corresponding X-ray diffraction peaks, the TiO_2 crystallite size was estimated using the Scherrer equation (Equation 2), where L is the average crystallite size in nm, λ is the wavelength of X-ray radiation (CuKα = 0.154056 nm), K is shape factor, taken as 0.9, β is the broadened profile width at half maximum height in radians and θ is the diffracting angle.

$$L = \frac{K\lambda}{\beta cos\theta} \quad (2)$$

2.4 Photocatalytic assays

2.4.1 Apparatus

196 Experiments were carried out in the annular FluHelik reactor (Espíndola et al., 2019; Moreira
197 et al., 2019) (Figure S1) consisting of an outer tube made of borosilicate glass (length =
198 196.0 mm, internal diameter = 65.6 mm; thickness = 1.8 mm) and an inner quartz sleeve
199 (external diameter = 23.0 mm; thickness = 1.0 mm) filled with an UVC lamp. The reactor is
200 equipped with one inlet and one outlet pipes (length = 43.0 mm, internal diameter = 7.0 mm)
201 located perpendicularly to the fluid flow and tangentially to the shell in horizontal plane and
202 at the top in opposite sides with 3.0 mm distance from reactor ends. The lamp employed was
203 a UVA Philips TL 6 W blacklight blue (λ_{max} = 365 nm) providing a photonic flow in the
204 annular reaction zone of 0.62 ± 0.02 W (Webler et al., 2019). The FluHelik photoreactor was
205 connected to a recirculated cylindrical glass vessel thermostatically controlled and
206 magnetically stirred.
207
208 *2.4.2 Experimental procedure*
209 The photocatalytic activity of the TiO_2/SBA-15 samples was evaluated for the
210 photodegradation of SDZ in the annular FluHelik reactor in multiple pass flow mode (batch
211 system). For this purpose, 1.5 L of a SDZ solution in pure water solution (PW) with $[SDZ]_0$
212 = 2 mg L^{-1} was stirred for 24 h (25 °C) with 150 mg of the photocatalyst, in the dark, to reach
213 the adsorption equilibrium. The resulting suspension was placed in the recirculation glass
214 vessel of the reactor, which was pumped to the FluHelik photoreactor by means of a gear
215 pump (Ismatec, model BVP-Z) at a flow rate of 75 L h^{-1}. In all the experiments, the
216 temperature set-point of the refrigerated thermostatic bath was adjusted to keep the solution
217 at 25 °C, and the initial pH was adjusted to 7.0 (after spiking with SDZ) using either H_2SO_4
218 or NaOH solutions (1.0 mol L^{-1}), but was not corrected over time. After switching on the
219 lamp, aliquots of 10 mL of the aqueous suspensions were collected from the recirculation
220 tank and filtered through a 0.45 µm membrane filter to remove the catalyst powder for

221 further HPLC analysis. The SDZ concentration was monitored by reversed-phase HPLC
222 using a VWR Hitachi ELITE LaChrom apparatus. Details of the analytical system are given
223 as Supplementary Information (SI).
224 Control experiments with non-modified SBA-15 and with standard TiO_2-P25 were also
225 carried out in the same conditions, as well as in the absence of any catalyst. The pseudo-
226 first-order kinetic constants for SDZ concentration decay (k_{SDZ}) in min^{-1} was calculated by
227 a nonlinear regression method according to Equation 3, where $[SDZ]_t$ and $[SDZ]_0$ are the
228 concentrations of SDZ at time t and $t = 0$, respectively.
229 $$[SDZ]_t = [SDZ]_0 \times e^{-k_{SDZ}t} \quad (3)$$
230 The material that demonstrated the best photocatalytic performance in the previous
231 experiments was chosen for the evaluation of the effect of catalyst mass (50, 150, 200, 300,
232 500 and 600 mg).
233 Reusability tests were performed for the best catalyst dose during 4 consecutive cycles. At
234 the end of each cycle, the spent catalyst was filtered off and oven-dried for 24 h (50 °C)
235 before being used for the next run with a fresh SDZ solution.
236 The matrix effect was evaluated using a real UWW (Table S1) spiked with 2 mg L^{-1} of SDZ.
237 A control experiment was run in the SDZ-spiked UWW using standard TiO_2-P25 as
238 photocatalyst, in similar conditions, but replacing the 500 mg of 30% TiO_2/SBA-15 by 150
239 mg of P-25 (which contains the equivalent TiO_2 dosage).
240 A new SDZ-spiked UWW sample was prepared, as above, but with a lower concentration of
241 SDZ ([SDZ] = 40 μg L^{-1}), and irradiated in the same conditions (with 500 mg of 30%
242 TiO_2/SBA-15). In this experiment, only three aliquots (200 mL each) were collected for
243 analysis: (1) before catalyst addition; (2) after 24 hours in the dark (adsorption period); (3)
244 after 180 min irradiation (photodegradation period). SDZ was extracted from the aliquots by
245 solid-phase extraction (SPE). Briefly, the 200 mL aliquots were filtered (0.45 μm polyamide

246 filters) and passed through 500 mg Oasis HLB cartridges (Waters). After washing and drying
247 the cartridge, the analyte was recovered in 10 mL of methanol. Due to the low SDZ
248 concentration, a more accurate detection system was necessary. The methanolic extracts
249 were then analyzed for SDZ content at the Institute of Research on Chemical and Biological
250 Analysis (IAQBUS) of the University of Santiago de Compostela, using a Liquid
251 Chromatography-triple quadrupolote-Tandem Mass Spectrometry (LC-QQQ-MS/MS)
252 system. More details about the instrumental setup are given in the SI file. Besides SDZ, the
253 samples were also screened for further CECs that were originally present in the UWW
254 sample by LC-high-resolution-quadrupole-time of flight mass spectrometer (LC-QTOF) as
255 detailed in the SI. In this way it was possible to preliminarily evaluate, both the adsorption
256 and photocatalytic potential of 30% TiO_2/SBA-15 for the removal of other CECs. More
257 experimental details are given in the SI file.
258
259 **3. Results and Discussion**
260 *3.1. Characterization of the photocatalyst materials*
261 Wide-angle diffraction patterns of the synthesized catalysts confirm the formation of
262 crystalline TiO_2 (Figure 1A). Pristine SBA-15 shows only a broad peak centered at $2\theta = 20°$,
263 corresponding to amorphous silica. In the presence of TiO_2, new diffraction peaks appear at
264 $2\theta = 25.3°$, 37.8°, 48.1°, 55.2° and 62.5°, which become more intense with the increase in
265 TiO_2 content. The observed diffraction pattern corresponds to the anatase phase of TiO_2
266 (JCPDS card n° 21-1272, space group *I41/amd*). The peaks correspond to (101), (004),
267 (200), (105) and (204) lattice planes of anatase, respectively. Diffraction peaks due to rutile
268 were not observed, evidencing that anatase was the only TiO_2 phase formed. The average
269 crystallite sizes *L*, as obtained from the Scherrer equation assuming spherical particles

(Equation 2), range between 6-8 nm (Table S2), which favors the photocatalytic activity (Van Grieken et al., 2002).

SAXS patterns of SBA-15 and of the TiO_2/SBA-15 catalysts (Figure 1B) show the typical reflections of 2D-hexagonal mesostructures (space group *p6mm*), showing that the mesoporous framework survived the functionalization procedure. Five well-resolved diffraction peaks can be seen in the 2θ range 0.5-3.0°, which can be indexed as the (100), (110), (200), (210) and (300) reflections. The hexagonal lattice parameter a_0 (which corresponds to the center-to-center pore distance) can be obtained from the d_{100} spacing using Equation 1, and is given in Table S2. A slight contraction of the silica framework in the TiO_2/SBA-15 samples can be observed, which can be attributed to the calcination at 700 °C to form TiO_2 particles.

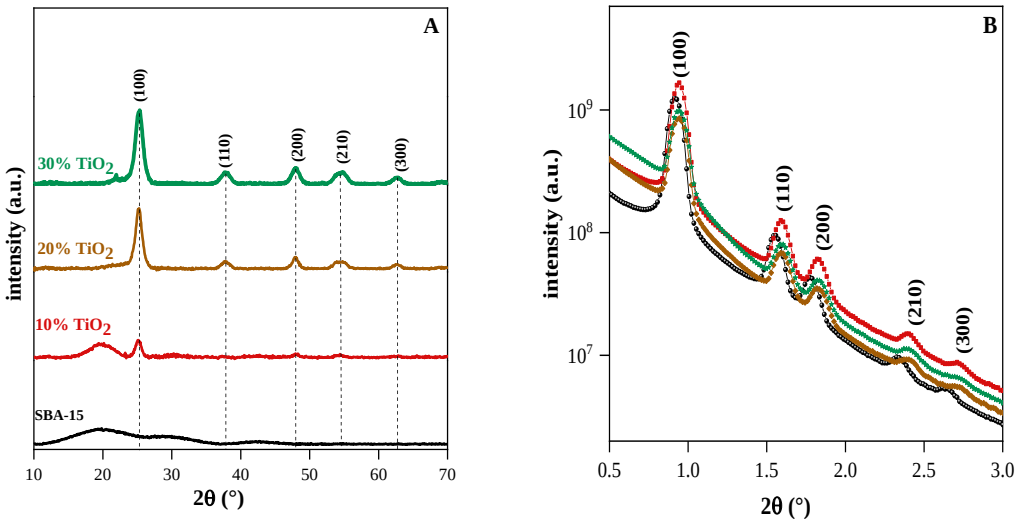

Figure 1. (A) Wide-angle XRD patterns of SBA-15 and TiO_2/SBA-15 catalysts. (B) Small-angle XRD patterns of SBA-15 (–●–); 10% TiO_2/SBA-15 (–■–); 20% TiO_2/SBA-15 (–◆–); 30% TiO_2/SBA-15 (–★–).

HRTEM images of SBA-15 and TiO_2/SBA-15 are shown in Figure 2 (additional images are given in Figure S2). Pristine SBA-15 presented the expected hexagonal array of parallel 1D

channels (Figure 2A, B) (Zhao et al., 1998). In contrast, the images of the TiO_2/SBA-15 materials (Figure 2C, E, G) showed TiO_2 NP decorating most of the surface of the SBA-15 particles. The observed surface coating could account for the disappearance of the amorphous silica band ($2\theta = 20°$) in the XRD pattern (Figure 1A). Some of the NP appear to be inside the pores, although their precise location cannot be ascertained. Moreover, some parts of the surface were not covered by the NP, revealing the naked SBA-15 structure underneath. This finding confirms that the SBA-15 matrix resisted the post-synthesis modification with TiO_2, which is in agreement with the SAXS measurements (Figure 1B).

The high magnification HRTEM images of the TiO_2/SBA-15 materials (Figure 2D, F, H) revealed individual TiO_2 NP on the surface. The diameters calculated from the TEM images for the NPs were 8.1 ± 2.2 nm (10% TiO_2/SBA-15), 10.5 ± 2.6 nm (20% TiO_2/SBA-15) and 7.6 ± 1.6 nm (30% TiO_2/SBA-15), which in general agree with the values determined by the Scherrer equation (Table S2). Some of the NP show clear diffraction patterns, with a *d*-spacing compatible with that calculated from the (101) diffraction peak (Figure 1A) at $2\theta = 25.3°$ ($d_{101} = 3.5$ Å).

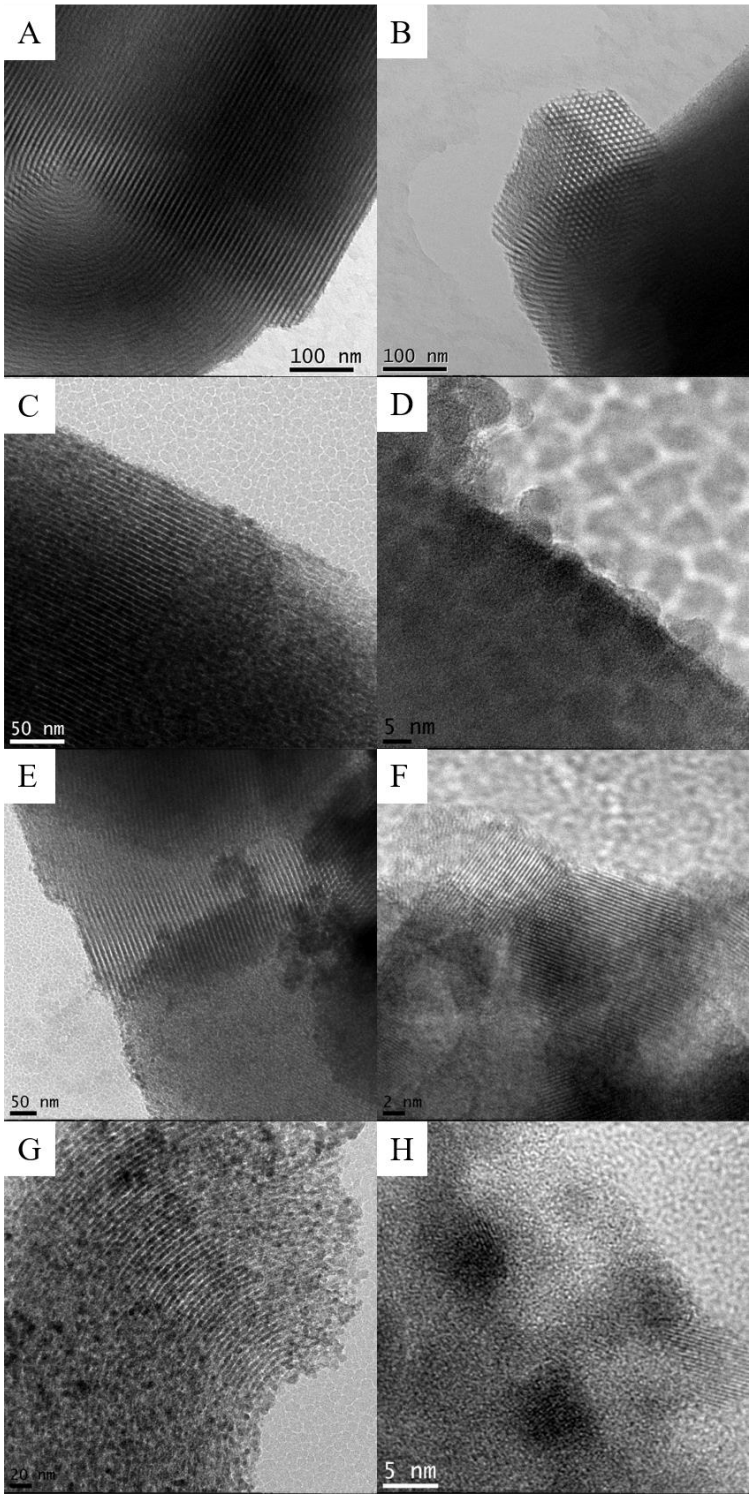

Figure 2. HRTEM images of pristine SBA-15 (A, B), 10% TiO_2/SBA-15 (C, D), 20% TiO_2/SBA-15 (E, F) and 30% TiO_2/SBA-15 (G, H).

The TiO_2/SBA-15 samples were further characterized by nitrogen adsorption isotherms (Figure 3A). The corresponding pore size distributions are shown in the insert of Figure 3A.

Textural parameters are given in Table S2. All the materials presented type IV(a) isotherms with H1 hysteresis loop, which are typical of 2D-hexagonal SBA-15 materials (Zhao et al., 1998). The data in Table S2 suggest that the TiO_2 NP were mainly attached to the external surface of the SBA-15 particles, as seen in the TEM images (Figure 2), since specific surface areas, pore volumes and pore diameters did not decrease substantially in comparison with SBA-15, as would be expected if the NP were inside the pores. The surface areas and pore volumes actually increased, which is likely due to the extra external area impinged by the presence of the coating NP. The large surface areas are beneficial for contaminant molecules to access the exposed active sites, thus favoring photocatalytic performance.

The presence of TiO_2 in the samples was further detected in the powder diffuse reflectance spectra of the catalysts (Figure 3B). The spectra show the typical UV absorption band of TiO_2, which is not seen in the spectrum of SBA-15. The spectra end at about 415 nm, corresponding to a bandgap energy of 3.0 eV, and are shifted to longer wavelengths compared to the TiO_2-P25 spectrum, showing that the absorption of UVA radiation by the synthesized TiO2/SBA-15 materials is favored.

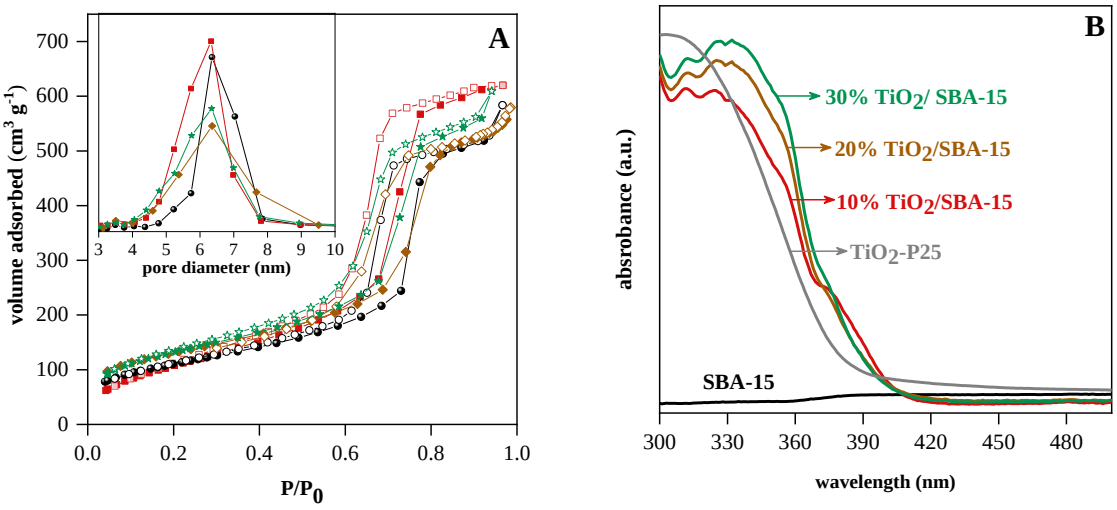

Figure 3. (A) Nitrogen adsorption isotherms of the TiO_2/SBA-15 catalysts. Inset: Pore size distributions (BJH from adsorption branches). Data for pristine SBA-15 are included for comparison. SBA-15 (–●–); 10% TiO_2/SBA-15 (–■–); 20% TiO_2/SBA-15 (–◆–); 30%

328 TiO_2/SBA-15 (−★−). (B) Absorbance spectra (from diffuse reflectance measurements) of
329 the SBA-15, TiO_2-P25 and TiO_2/SBA-15 catalysts.

330 *3.2 Photocatalytic activity*

331 *3.2.1 Effect of TiO_2 content on SDZ degradation*

332 The photocatalytic activity of the TiO_2/SBA-15 materials was monitored using SDZ as a
333 model CEC. Figure 4 shows the influence of the TiO_2 content on the SDZ degradation
334 kinetics, and the results of the experiments are summarized in Table 2. Note that direct
335 photolysis of SDZ, in homogeneous solution, was almost negligible, reaching only 1.6% of
336 SDZ degradation after 180 min (Table 2). When the non-functionalized SBA-15 was present,
337 ca 14% of the SDZ was removed by adsorption, and only 3% of the SDZ was removed by
338 photodegradation. In the presence of TiO_2, however, most of the SDZ was removed by
339 photocatalysis, rather than adsorption; in fact, only 2-6% of the SDZ was adsorbed on the
340 TiO_2/SBA-15 materials. The photocatalytic degradation of SDZ, on the other hand,
341 increased with TiO_2 content from 32% (10% TiO_2/SBA-15) to 65% (20% TiO_2/SBA-15)
342 and to 73% (30% TiO_2/SBA-15). Reaction rates also increased with increasing TiO_2 content.
343 A four-fold increase in the pseudo-first order kinetic constant was observed as going from
344 10% to 30% TiO_2 (Table 2).

345 A relevant issue is whether the SDZ is deactivated by the irradiation treatment, forming
346 decomposition products with no capability of inducing bacterial resistance. The
347 photocatalytic degradation of SDZ and other sulfonamides over TiO_2 has been studied by
348 several authors (Baran et al., 2009; Batista et al., 2014; Calza et al., 2004; Castanheira et al.,
349 2018; Huang et al., 2015; Liu et al., 2018). The main pathway reported begins with the
350 breakdown of the S−N bond, followed by secondary fragmentation reactions. Baran *et al*
351 (Baran et al., 2006) and Zessel *et al* (Zessel et al., 2014) have shown that the photolytic
352 products of SDZ degradation were devoid of antibacterial activity, and therefore could not

cause bacterial resistance. Moreover, those reports suggest that total mineralization is not necessary for SDZ deactivation. The characterization of the degradation products, however, is out of the scope of the present work.

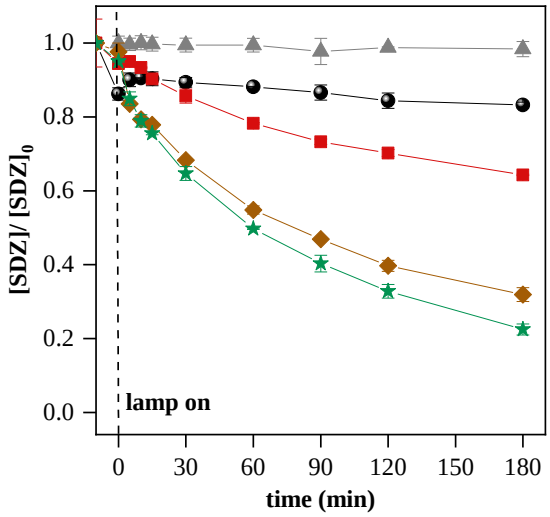

Figure 4. Photolysis (–▲–), and the photocatalytic performance of SBA-15 (–●–), 10% TiO_2/SBA-15 (–■–), 20% TiO_2/SBA-15 (–◆–) and 30% TiO_2/SBA-15 (–★–) for SDZ photodegradation in the FluHelik photoreactor. Conditions: $m_{photocat}$ = 150 mg; V_{sol} = 1.5 L; $[SDZ]_0$ = 1.88 ± 0.11 mg L^{-1}; pH_0 = 7.0; T = 25 °C. Time values below zero represent the adsorption time in the dark (prior turning on the lamp) and are out of scale (the actual adsorption time was 24 hours).

3.2.2 Effect of the mass of catalyst employed

Considering that 30% TiO_2/SBA-15 showed the best photocatalytic performance among the three samples, this material was selected for further experiments. Figure 5 shows the effect of varying the mass of 30% TiO_2/SBA-15 catalyst on SDZ photodegradation. Table 2 shows the corresponding parameters obtained from the experiments. The adsorption of SDZ increased with the increase in the catalyst content, reaching the limiting value of 8% SDZ adsorption. Furthermore, photocatalytic performance was also improved, with the best

performance obtained for 500 mg of the 30% TiO_2/SBA-15 catalyst, resulting in complete SDZ removal after 120 min of irradiation. A further increase in catalyst mass did not result in a better performance (Figure 5), both in terms of removal percentage and removal rate, which can be attributed to the increasing turbidity of the suspensions, partially blocking the penetration of the radiation.

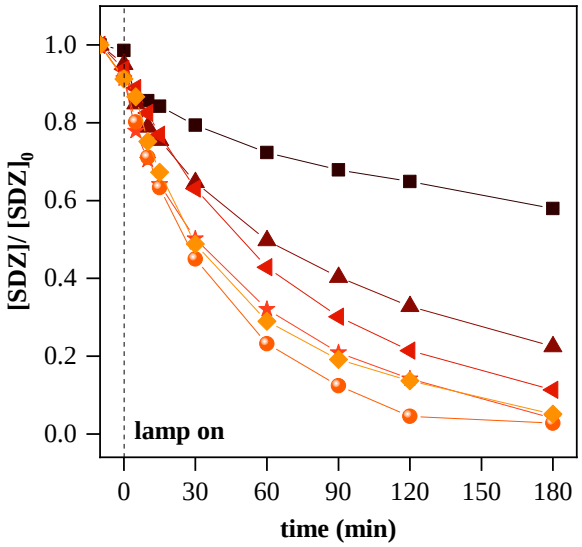

Figure 5. Photocatalytic performance of 50 mg (—■—), 150 mg (—▲—), 200 mg (—◀—), 300 mg (—★—), 500 mg (—●—) and 600 mg (—◆—) of 30% TiO_2/SBA-15 for SDZ photodegradation in the FluHelik photoreactor. Conditions: V_{sol} = 1.5 L; $[SDZ]_0$ = 1.88 ± 0.11 mg L^{-1}; pH_0 = 7.0; T = 25 °C. Time values below zero represent the adsorption time in the dark (prior turning on the lamp) and are out of scale (the actual adsorption time was 24 hours).

3.2.3 Photocatalyst reutilization

From the previous results, the mass of 500 mg of the 30% TiO_2/SBA-15 catalyst was selected for the reutilization studies. Figure 6 shows SDZ photodegradation over three cycles with the selected sample, and Table 2 shows the corresponding parameters. As seen in Table 2,

388 the adsorptive capacity of the material decreased after the first cycle. This result may be an
389 indication that the remaining sulfadiazine, or intermediates formed during photodegradation
390 remain on the surface of the photocatalyst material after the end of the first cycle. The
391 photoactivity, however, remained high in the subsequent cycles, regardless of the lower
392 adsorption capacity. More than 90% of freshly added SDZ was photodegraded in the second
393 and third cycles, and with nearly the same rate constant as the first cycle (Table 2). The
394 possibility of reutilization is essential for any practical large-scale application.

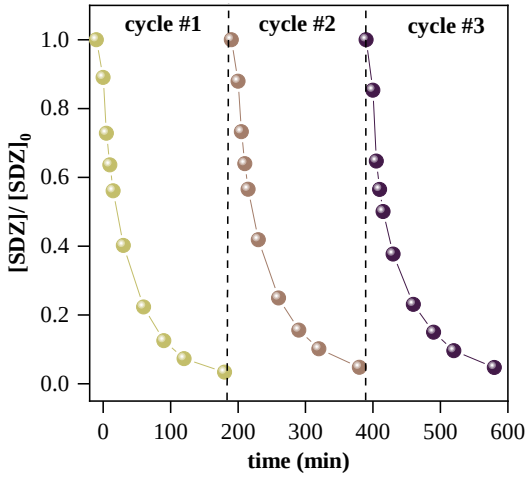

395

396 **Figure 6.** Reuse of 30% TiO_2/SBA-15 for SDZ photodegradation in a FluHelik photoreactor.
397 Conditions: $m_{photocat}$ = 500 mg; V_{sol} = 1.5 L; $[SDZ]_0$ = 1.88 ± 0.11 mg L^{-1}; pH_0 = 7.0; T = 25
398 °C.

399

400 3.*2.4 Performance of TiO_2/SBA-15 catalysts in urban wastewater matrix*

401 The degradation of SDZ was also evaluated using a sample of UWW (Table S1), spiked with
402 2 mg L^{-1} of SDZ. The best condition from the previous experiments, 30% TiO_2/SBA-15 (500
403 mg), was employed here. The photocatalytic performance of this sample was compared to
404 that of commercially available TiO_2-P25. As observed in Figure 7, TiO_2-P25 was more
405 efficient for SDZ degradation than 30% TiO_2/SBA-15 in PW. In the UWW, however, the

opposite behavior was observed, with TiO_2/SBA-15 showing better performance than TiO_2-P25. 56% SDZ degradation was obtained after 180 min, with 30% TiO_2/SBA-15 in the UWW, as compared to 32% SDZ degradation with TiO_2-P25 (Table 2). Moreover, SDZ degradation was faster with 30% TiO_2/SBA-15, as indicated by the rate constants in Table 2. These results may be due to the reported agglomeration of TiO_2-P25 NPs when suspended in wastewater samples, arising from the combined effect of high ionic strength and dissolved organic matter (Romanello and Cortalezzi, 2013; Zhou et al., 2015; Ren et al., 2017; Xu, 2018). Zhou et al. (2015), for example, showed that TiO_2 NPs with 21 nm diameter formed aggregates with sizes greater than 200 nm when dispersed in real wastewater samples. Thus, dispersion of the TiO_2 NP onto the SBA-15 support helped to avoid catalyst nanoparticles agglomeration, leading to a better performance than the standard TiO_2-P25 in the real water studied.

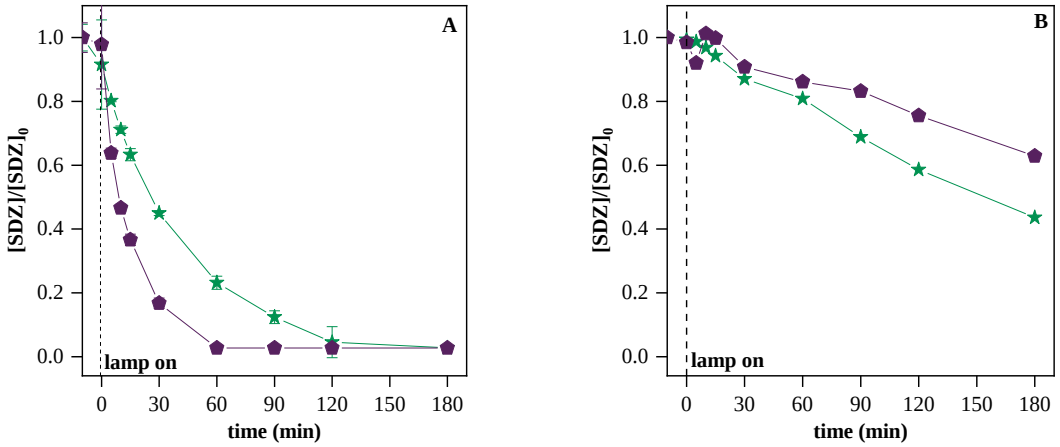

Figure 7. Comparison between 30% TiO_2/SBA-15 (–★–) and TiO_2-P25 (–⬟–) for SDZ photodegradation from (A) PW and (B) UWW matrices in the FluHelik photoreactor. Conditions: $m_{photocat}$ = 500 mg; V_{sol} = 1.5 L; $[SDZ]_0$ = 1.88 ± 0.11 mg L^{-1}; pH_0 = 7.0 (PW) and 7.5 (UWW); T = 25 °C. Time values below zero represent the adsorption time in the dark (prior turning on the lamp) and are out of scale (the actual adsorption time was 24 hours).

The SDZ concentration ($[SDZ]_0$ = 1.88 mg L^{-1}) employed in the optimization experiments reported above is much higher than the [SDZ] expected to be found in real wastewater. Therefore, a new SDZ-spiked UWW sample, with [SDZ] = 40 µg L^{-1}, was prepared and irradiated in the FluHelik, with 500 mg of 30% TiO_2/SBA-15 (other conditions as above). For this sample, although the adsorption was null, 90.0% of the SDZ was removed by photodegradation (Table 2, last entry), stressing the high efficiency of the present system in conditions similar to real conditions.

Table 2. Percentage of adsorption (% SDZ_{ads}), percentage of photodegradation (% SDZ_{deg}), pseudo-first order reaction rate constant (k_{SDZ}), determination coefficient (R^2) of the nonlinear data fit and initial reaction rate ($r_{0,SDZ}$) values obtained in the degradation experiments of SDZ with TiO_2/SBA-15 catalyst in the FluHelik photoreactor.

Experiment[a]	Matrix[b]	photocatalyst	$m_{photocat}$ (mg)	C_{TiO2} (mg L^{-1})	pH_f	%SDZ ads	%SDZ deg	k_{SDZ} (10^{-2} min^{-1})[c]	R^2
Homogeneous (photolysis)	PW	–	–	–	7.4	–	1.6	–	–
Heterogeneous (photocatalysis)	**Influence of TiO_2 content**								
	PW	SBA-15	150	0	7.4	13.8	3.1	0.05	0.97
	PW	10% TiO_2/SBA-15	150	15	7.4	5.6	31.6	0.20	0.96
	PW	20% TiO_2/SBA-15	150	30	7.2	2.4	65.2	0.61	0.99
	PW	30% TiO_2/SBA-15	150	45	7.4	4.9	73.2	0.81	0.99
	Effect of the mass of photocatalyst employed								
	PW	30% TiO_2/SBA-15	50	15	7.3	1.4	40.7	0.23	0.98
	PW	30% TiO_2/SBA-15	200	60	7.0	6.2	82.5	1.26	0.99
	PW	30% TiO_2/SBA-15	300	90	7.1	8.6	87.3	1.86	0.98
	PW	30% TiO_2/SBA-15	500	150	7.1	8.4	88.8	2.36	0.99
	PW	30% TiO_2/SBA-15	600	180	7.3	8.7	86.2	1.85	0.99
	Photocatalyst reutilization								
	PW	30% TiO_2/SBA-15 (1^{st} cycle)	500	150	7.2	9.7	87.3	1.87	0.99
	PW	30% TiO_2/SBA-15 (2^{nd} cycle)	500	150	7.1	2.7	94.5	1.72	0.99
	PW	30% TiO_2/SBA-15 (3^{rd} cycle)	500	150	7.3	3.1	94.0	1.66	0.99

Matrix influence								
PW	TiO_2-P25	150	150	6.6	2.2	95.0	6.09	0.99
UWW	TiO_2-P25	150	150	7.2	1.6	31.6	0.25	0.97
UWW	30% TiO_2/SBA-15	500	150	7.6	0.6 (0)[d]	56.4 (90.0)[d]	0.43	0.99

444 [a] Conditions: V_{sol} = 1.5 L; Irradiation range: 0-180 min; Q = 75 L h^{-1}; $[SDZ]_0$ = 2 mg L^{-1} (nominal value); pH_0 = 7.0 (PW), 7.5 (UWW). [b] PW: Pure water; UWW: Urban wastewater.

445 [c] Apparent first-order rate constant (k_{app}) of the photocatalytic SDZ degradation. [d] Data in parenthesis are for the experiment with $[SDZ]_0$ = 40 µg L^{-1} in UWW.

446 *3.2.5 Removal of other CECs from UWW*

447 The LC-QTOF screening (Castro et al., 2021; Wilson et al., 2021) allowed the detection
448 of 65 other CECs (Table S3), which were originally present in the UWW (not spiked in)
449 (Paíga et al., 2019; Schymanski et al., 2014). The CECs response was then determined in
450 the original UWW (before adding the catalyst), after 24 hours in contact with 500 mg of
451 30% TiO_2/SBA-15 and after irradiating the mixture in the FluHelik for 180 minutes, in
452 the presence of 30% TiO_2/SBA-15. The results are displayed in Figure 8, in the form of
453 radar charts (Paíga et al., 2019), where the contribution of adsorption and photocatalysis
454 for the removal of each drug can be easily visualized, as a percent of the original response
455 (A/A_0). More information is presented in Table S3. With these data, a fast screening can
456 be performed on the activity of TiO_2/SBA-15 for the removal of the different CECs, in a
457 single experiment.

458 In one hand some of the CECs adsorbed strongly onto the catalyst, but were not
459 photodegraded, and on the other hand, other CECs did not adsorb on the catalyst, but
460 were efficiently degraded by photocatalysis (Figure 8). Since the characterization of the
461 catalyst showed the TiO_2 NP to be located outside the SBA-15 particles, TiO_2/SBA-15
462 presumably acts as a dual-action material for CECs removal, with independent adsorption
463 (mesopores) and photocatalytic (NP) sites.

464 The list of CECs found in UWW includes predominantly pharmaceutical drugs used for
465 the neurological system, whose results are displayed in Figure 8A. It is worth noting that
466 around 70% of neurological drugs were reduced to less than 50% of the original
467 concentration, after adsorption followed by photocatalysis in the FluHelik reactor.

468 Drugs used as anti-infective and antibacterial agents (Figure 8B), such as clarithromycin
469 (CR), sulfapyridine (SPy), sulfamethoxazole (SMX), levofloxacin (LVX) and
470 trimethoprim (TMP), did not show adsorption affinity for the surface of the TiO_2/SBA-

15 catalyst (similarly to SDZ), the same occurring with the cardiovascular drugs losartan (LOS), perindopril (PRD), propranolol (PRN), sotalol (STL), and telmisartan (TEL). However, most of these drugs were efficiently removed after photocatalysis (except for SMX), with nearly complete photodegradation in some cases (SPy, TMP, PRN) (Figure 8B).

Drugs for dermatological use (Figure 8C) such as climbazole (CLZ) and fluconazole (II) (FLC), and substances which are not part of the drug class − fipronil (FIP), nitrophenolate (NP), ritalinic acid (RA), sucralose (SUC), terbutrin (TB), and toluene 2-sulfonamide (TSN), were also not adsorbed on the surface of 30% TiO_2/SBA-15, and were only partially degraded after photocatalysis. On the other hand, thiemonium (TI), sitagliptin (SGN), levorphanol (LEV), denatonium (DE), and dietiltoluamide (DEET), which are drugs used for other treatments, were completely eliminated after 180 min of irradiation (Figure 8C).

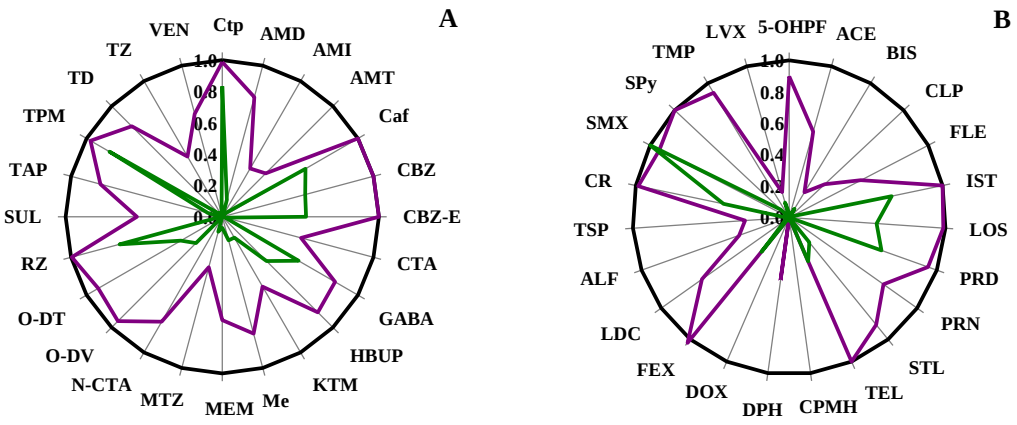

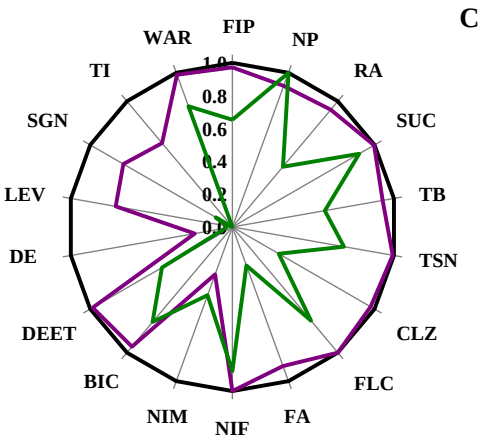

484 **Figure 8.** Radar charts of the response ratios (A/A_0) initially present (——) and after
485 adsorption (——) and photocatalysis in the presence of 30% TiO_2/SBA-15 (——), for all
486 detected CECs. (A) Pharmaceuticals for nervous system. (B) Antibiotics and
487 pharmaceuticals for cardiovascular, respiratory and urinary system. (C) Pharmaceuticals
488 for dermatological treatment and other contaminants.

489

490 **Conclusions**

491 The combination of the FluHelik photoreactor with the TiO_2/SBA-15 photocatalyst
492 synthesized in this work was shown to be very promising for the removal of CECs present
493 in UWW. The TiO_2/SBA-15 samples were synthesized by the sol-gel post-synthetic
494 method and subsequently characterized by a collection of techniques, such as XRD,
495 SAXS, TEM, nitrogen adsorption-desorption and UV-Vis DRS. Among all candidate
496 catalysts, 30% TiO_2/SBA-15 showed the highest catalytic performance under optimal
497 conditions. Moreover, the 30% TiO_2/SBA-15 sample was more efficient than standard
498 TiO_2-P25 for SDZ degradation in UWW, showing that supporting the TiO_2 NPs on SBA-
499 15 effectively inhibited TiO_2 agglomeration in this high ionic strength matrix.
500 Furthermore, the FluHelik + 30% TiO_2/SBA-15 combination was able to remove 90% of
501 the SDZ when spiked at concentrations in the µg L^{-1} range, similar to SDZ concentrations

found in the environment. Additionally, tens of other pharmaceutical drugs detected in the UWW sample studied here were also partially or totally removed from the UWW using the FluHelik + 30% TiO_2/SBA-15 system.

Acknowledgements

SB and ACSCT acknowledge the São Paulo Research Foundation (FAPESP) for the financial support (grants #2016/05496-2 and #2018/21271-6, respectively). BC thanks the National Council for Scientific and Technological Development (CNPq) (grant #204891/2018-3) for supporting the interchange research period at Faculty of Engineering University of Porto (Portugal). ACSCT also thanks the National Council for Scientific and Technological Development (CNPq) (grant #307481/2017-4). The authors thank the Multiuser Central Facilities (UFABC) for the analytical support. This work was also financially supported by the i) Base Funding - UIDB/50020/2020 of the Associate Laboratory LSRE-LCM - funded by national funds through FCT/MCTES (PIDDAC); ii) the European Regional Development Fund (ERDF) through the Interreg V-A Spain-Portugal Programme (POCTEP) 2014-2020 (ref. 0725_NOR_WATER_1_P). Vítor J.P. Vilar acknowledges the FCT Individual Call to Scientific Employment Stimulus 2017 (CEECIND/01317/2017). The team of the University of Santiago acknowledges funding by Xunta de Galicia (ED431C2017), the Spanish Agencia Estatal de Investigación (ref. CTM2017-84763-C3-R-2), partly cofounded by the ERDF.

References

Acosta-Silva, Y.J., Nava, R., Hernández-Morales, V., Macías-Sánchez, S.A., Gómez-Herrera, M.L., Pawelec, B., 2011. Methylene blue photodegradation over titania-decorated SBA-15. Appl. Catal. B Environ. 110, 108–117. https://doi.org/10.1016/j.apcatb.2011.08.032

Alfonso-Muniozguren, P., Gomes, A.I., Saroj, D., Vilar, V.J.P., Lee, J., 2021. The role of ozone combined with UVC/H_2O_2 process for the tertiary treatment of a real slaughterhouse wastewater. J. Environ. Manage. 289, 112480. https://doi.org/10.1016/j.jenvman.2021.112480

Araújo, M.M., Silva, L.K.R., Sczancoski, J.C., Orlandi, M.O., Longo, E., Santos, A.G.D., Sá, J.L.S., Santos, R.S., Luz, G.E., Cavalcante, L.S., 2016. Anatase TiO_2 nanocrystals anchored at inside of SBA-15 mesopores and their optical behavior. Appl. Surf. Sci. 389, 1137–1147. https://doi.org/10.1016/j.apsusc.2016.08.018

Balakrishnan, V.K., Terry, K.A., Toito, J., 2006. Determination of sulfonamide antibiotics in wastewater: A comparison of solid phase microextraction and solid phase extraction methods. J. of Chromat. A 1131, 1–10. https://doi.org/10.1016/j.chroma.2006.07.011

Baran, W., Adamek, E., Sobczak, A., Makowski, A., 2009. Photocatalytic degradation of sulfa drugs with TiO_2, Fe salts and TiO_2/$FeCl_3$ in aquatic environment-Kinetics and degradation pathway. Appl. Catal. B Environ. 90, 516–525. https://doi.org/10.1016/j.apcatb.2009.04.014

Baran, W., Adamek, E., Ziemiańska, J., Sobczak, A., 2011. Effects of the presence of sulfonamides in the environment and their influence on human health. J. Hazard. Mater. 196, 1–15. https://doi.org/10.1016/j.jhazmat.2011.08.082

Baran, W., Sochacka, J., Wardas, W., 2006. Toxicity and biodegradability of

sulfonamides and products of their photocatalytic degradation in aqueous solutions. Chemosphere 65, 1295–1299. https://doi.org/10.1016/j.chemosphere.2006.04.040

Barbosa, I.D., Moreira, F.C., Silva, T.F.C. V, Webler, A.D., Boaventura, R.A.R., Vilar, V.J.P., 2020. Development of a treatment train for the remediation of a hazardous industrial waste land fill leachate: A big challenge. Sci. Total Environ. 741, 140165. https://doi.org/10.1016/j.scitotenv.2020.140165

Batista, A.P.S., Pires, F.C.C., Teixeira, A.C.S.C., 2014. Photochemical degradation of sulfadiazine, sulfamerazine and sulfamethazine: Relevance of concentration and heterocyclic aromatic groups to degradation kinetics. J. Photochem. Photobiol. A Chem. 286, 40–46. https://doi.org/10.1016/j.jphotochem.2014.04.022

Besançon, M., Michelin, L., Josien, L., Vidal, L., Assaker, K., Bonne, M., Lebeau, B., Blin, J.L., 2016. Influence of the porous texture of SBA-15 mesoporous silica on the anatase formation in TiO_2-SiO_2 nanocomposites. New J. Chem. 40, 4386–4397. https://doi.org/10.1039/c5nj02859k

Busuioc, A.M., Meynen, V., Beyers, E., Mertens, M., Cool, P., Bilba, N., Vansant, E.F., 2006. Structural features and photocatalytic behaviour of titania deposited within the pores of SBA-15. Appl. Catal. A Gen. 312, 153–164. https://doi.org/10.1016/j.apcata.2006.06.043

Calza, P., Medana, C., Pazzi, M., Baiocchi, C., Pelizzetti, E., 2004. Photocatalytic transformations of sulphonamides on titanium dioxide. Appl. Catal. B Environ. 53, 63–69. https://doi.org/10.1016/j.apcatb.2003.09.023

Calzada, L.A., Castellanos, R., García, L.A., Klimova, T.E., 2019. TiO_2, SnO_2 and ZnO catalysts supported on mesoporous SBA-15 versus unsupported nanopowders in photocatalytic degradation of methylene blue. Microporous Mesoporous Mater. 285, 247–258. https://doi.org/10.1016/j.micromeso.2019.05.015

577 Castanheira, B., Triboni, E.R., Andrade, L.S., Trindade, F.J., Otubo, L., Teixeira,
578 A.C.S.C., Politi, M.J., Queiroz, T.B., Brochsztain, S., 2018. Synthesis of novel
579 periodic mesoporous organosilicas containing 1,4,5,8-naphthalenediimides within
580 the pore walls and their reduction to generate wall-embedded free radicals. Langmuir
581 34, 8195–8204. https://doi.org/10.1021/acs.langmuir.8b00220
582 Castro, V., Quintana, J.B., Carpinteiro, I., Cobas, J., Carro, N., Cela, R., Rodil, R., 2021.
583 Combination of different chromatographic and sampling modes for high-resolution
584 mass spectrometric screening of organic microcontaminants in water. Anal. Bioanal.
585 Chem. https://doi.org/10.1007/s00216-021-03226-6
586 Conceição, D.S., Graça, C.A.L., Ferreira, D.P., Ferraria, A.M., Fonseca, I.M., Botelho do
587 Rego, A.M., Teixeira, A.C.S.C., Vieira Ferreira, L.F., 2017. Photochemical insights
588 of TiO_2 decorated mesoporous SBA-15 materials and their influence on the
589 photodegradation of organic contaminants. Microporous Mesoporous Mater. 253,
590 203–214. https://doi.org/10.1016/j.micromeso.2017.07.013
591 Dong, H., Zeng, G., Tang, L., Fan, C., Zhang, C., He, X., He, Y., 2015. An overview on
592 limitations of TiO_2-based particles for photocatalytic degradation of organic
593 pollutants and the corresponding countermeasures. Water Res. 79, 128–146.
594 https://doi.org/10.1016/j.watres.2015.04.038
595 Espíndola, J.C., Cristóvão, R.O., Araújo, S.R.F., Neuparth, T., Santos, M.M., Montes, R.,
596 Quintana, J.B., Rodil, R., Boaventura, R.A.R., Vilar, V.J.P., 2019. An innovative
597 photoreactor, FluHelik, to promote UVC/H_2O_2 photochemical reactions: Tertiary
598 treatment of an urban wastewater. Sci. Total Environ. 667, 197–207.
599 https://doi.org/10.1016/j.scitotenv.2019.02.335
600 Espíndola, J.C., Vilar, V.J.P., 2020. Innovative light-driven chemical/catalytic reactors
601 towards contaminants of emerging concern mitigation : A review. Chem. Eng. J. 394,

124865. https://doi.org/10.1016/j.cej.2020.124865

Espíndola, J.C., Caianelo, M., Scaccia, N., Rodrigues-Silva, C., Guimarães, J.R. Vilar, V.J.P., 2021. Trace organic contaminants removal from municipal wastewater using the FluHelik reactor: From laboratory-scale to pre-pilot scale. J. Environ. Chem. Eng. 9, 105060. https://doi.org/10.1016/j.jece.2021.105060

Fagan, R., Mccormack, D.E., Dionysiou, D.D., Pillai, S.C., 2016. A Review of Solar and Visible Light Active TiO_2 Photocatalysis for Treating Bacteria, Cyanotoxins and Contaminants of Emerging. Concern. Mater. Sci. Semicond. Process. 42, 2–14. https://doi.org/10.1016/j.mssp.2015.07.052

García-Galán, M.J., Díaz-Cruz, M.S., Barceló, D., 2011. Occurrence of sulfonamide residues along the Ebro river basin Removal in wastewater treatment plants and environmental impact assessment. Environ. Int. 37, 462–473. https://doi.org/10.1016/j.envint.2010.11.011

Gomes, A.I., Souza-Chaves, B.M., Park, M., Silva, T.F.C.V., Boaventura, R.A.R. Vilar, V.J.P., 2021. How does the pre-treatment of land fill leachate impact the performance of O_3 and O_3/UVC processes? Chemosphere 278, 130389. https://doi.org/10.1016/j.chemosphere.2021.130389

Gomes, A.I., Foco, M.L.R., Vieira, E., Cassidy, J., Silva, T.F.C.V., Fonseca, A., Saraiva, I., Boaventura, R.A.R., Vilar, V.J.P., 2018. Multistage treatment technology for leachate from mature urban land fill: Full scale operation performance and challenges. Chem. Eng. J. 376, 120573. https://doi.org/10.1016/j.cej.2018.12.033

Huang, X., Feng, Y., Hu, C., Xiao, X., Yu, D., Zou, X., 2015. Mechanistic QSAR models for interpreting degradation rates of sulfonamides in UV-photocatalysis systems. Chemosphere 138, 183–189. https://doi.org/10.1016/j.chemosphere.2015.05.075

626 Kovalakova, P., Cizmas, L., Mcdonald, T.J., Blahoslav, M., Feng, M., Sharma, V.K.,
627 2020. Occurrence and Toxicity of Antibiotics in the Aquatic Environment : A
628 Review. Chemosphere 251, 126351.
629 https://doi.org/10.1016/j.chemosphere.2020.126351

630 Krzeminski, P., Concetta, M., Karaolia, P., Langenhoff, A., Almeida, C.M.R., Felis, E.,
631 Gritten, F., Rasmus, H., Fernandes, T., Manaia, C.M., Rizzo, L., Fatta-kassinos, D.,
632 2019. Performance of secondary wastewater treatment methods for the removal of
633 contaminants of emerging concern implicated in crop uptake and antibiotic resistance
634 spread : A review. Sci. Total Environ. 648, 1052–1081.
635 https://doi.org/10.1016/j.scitotenv.2018.08.130

636 Kümmerer, K., 2009a. Antibiotics in the aquatic environment – A review – Part I.
637 Chemosphere 75, 417–434. https://doi.org/10.1016/j.chemosphere.2008.11.086

638 Kümmerer, K., 2009b. Antibiotics in the aquatic environment – A review – Part II.
639 Chemosphere 75, 435–441. https://doi.org/10.1016/j.chemosphere.2008.12.006

640 Lachheb, H., Ahmed, O., Houas, A., Nogier, J.P., 2011. Photocatalytic activity of TiO_2–
641 SBA-15 under UV and visible light. J. Photochem. Photobiol. A Chem. 226, 1–8.
642 https://doi.org/10.1016/j.jphotochem.2011.09.017

643 Liou, T.H., Hung, L.W., Liu, C.L., Zhang, T.Y., 2018. Direct synthesis of nano titania on
644 highly-ordered mesoporous SBA-15 framework for enhancing adsorption and
645 photocatalytic activity. J. Porous Mater. 25, 1337–1347.
646 https://doi.org/10.1007/s10934-017-0544-5

647 Liu, C., Lin, X., Li, Y., Xu, P., Li, M., Chen, F., 2016. Enhanced photocatalytic
648 performance of mesoporous TiO_2 coated SBA-15 nanocomposites fabricated through
649 a novel approach : supercritical deposition aided by liquid-crystal template. Mater.
650 Res. Bull. 75, 25–34. https://doi.org/10.1016/j.materresbull.2015.10.052

Liu, X., Liu, Y., Lu, S., Guo, W., Xi, B., 2018. Performance and mechanism into TiO_2/Zeolite composites for sulfadiazine adsorption and photodegradation. Chem. Eng. J. 350, 131–147. https://doi.org/10.1016/j.cej.2018.05.141

López-Muñoz, M.J., Grieken, R.V., Aguado, J., Marugán, J., 2005. Role of the support on the activity of silica-supported TiO_2 photocatalysts: Structure of the TiO_2/SBA-15 photocatalysts. Catal. Today 101, 307–314. https://doi.org/10.1016/j.cattod.2005.03.017

Mehta, A., Mishra, A., Sharma, M., Singh, S., Basu, S., 2016. Effect of silica/titania ratio on enhanced photooxidation of industrial hazardous materials by microwave treated mesoporous SBA-15/TiO_2 nanocomposites. J. Nanoparticle Res. 18, 1–9. https://doi.org/10.1007/s11051-016-3523-x

Miranda-García, N., Maldonado, M.I., Coronado, J.M., Malato, S., 2010. Degradation study of 15 emerging contaminants at low concentration by immobilized TiO_2 in a pilot plant. Catal. Today 151, 107–113. https://doi.org/10.1016/j.cattod.2010.02.044

Miranda-García, N., Suárez, S., Maldonado, M.I., Malato, S., Sánchez, B., 2014. Regeneration approaches for TiO_2 immobilized photocatalyst used in the elimination of emerging contaminants in water. Catal. Today 230, 27–34. https://doi.org/10.1016/j.cattod.2013.12.048

Mohammad, A.B., Zhou, J.L., Ngo, H.H., Guo, W., Thomaidis, N.S., Xu, J. 2017. Progress in the biological and chemical treatment technologies for emerging contaminant removal from wastewater: A critical review. J. Hazard. Mater. 323, 274–298. https://doi.org/10.1016/j.jhazmat.2016.04.045

Moreira, F.C., Bocos, E., Faria, A.G.F., Pereira, J.B.L., Fonte, C.P., Santos, R.J., Carlos, J., Lopes, B., Dias, M.M., Sanromán, M.A., Pazos, M., Boaventura, R.A.R., Vilar, V.J.P., 2019. Selecting the best piping arrangement for scaling-up an annular channel

reactor: An experimental and computational fluid dynamics study. Sci. Total Environ. 667, 821–832. https://doi.org/10.1016/j.scitotenv.2019.02.260

Paíga, P., Correia, M., Fernandes, M.J., Silva, A., Carvalho, M., Vieira, J., Jorge, S., Silva, J.G., Freire, C., Delerue-Matos, C., 2019. Assessment of 83 pharmaceuticals in WWTP influent and effluent samples by UHPLC-MS/MS: Hourly variation. Sci. Total Environ. 648, 582–600. https://doi.org/10.1016/j.scitotenv.2018.08.129

Paulus, G.K., Hornstra, L.M., Alygizakis, N., Slobodnik, J., Thomaidis, N., Medema, G., 2019. The impact of on-site hospital wastewater treatment on the downstream communal wastewater system in terms of antibiotics and antibiotic resistance genes. Int. J. Hyg. Environ. Health 222, 635–644. https://doi.org/10.1016/j.ijheh.2019.01.004

Ren, M., Horn, H., Frimmel, F.H., 2017. Aggregation behavior of TiO_2 nanoparticles in municipal effluent: Influence of ionic strengthen and organic compounds. Water Res. 123, 678–686. https://dx.doi.org/10.1016/j.watres.2017.07.021

Rivera-Utrilla, J., Sánchez-Polo, M., Ferro-García, M.Á., Prados-Joya, G., Ocampo-Pérez, R., 2013. Pharmaceuticals as emerging contaminants and their removal from water. A review. Chemosphere. 93, 1268–1287 https://doi.org/10.1016/j.chemosphere.2013.07.059

Rodriguez-Narvaez, O.M., Peralta-Hernandez, J.M., Goonetilleke, A., Bandala, E.R., 2017. Treatment technologies for emerging contaminants in water: A review. Chem. Eng. J. 323, 361–1380 https://doi.org/10.1016/j.cej.2017.04.106

Romanello, M.B., Cortalezzi, M.M.F., 2013. An experimental study on the aggregation of TiO_2 nanoparticles under environmentally relevant conditions. Water Res. 47, 3887–3898 https://dx.doi.org/10.1016/j.watres.2012.11.061

Salameh, C., Nogier, J.-P., Launay, F., Boutros, M., 2015. Dispersion of colloidal TiO_2

nanoparticles on mesoporous materials targeting photocatalysis applications. Catal. Today 257, 35–40. https://doi.org/10.1016/j.cattod.2015.03.025

Schymanski, E.L., Jeon, J., Gulde, R., Fenner, K., Ruff, M., Singer, H.P., Hollender, J., 2014. Identifying small molecules via high resolution mass spectrometry: Communicating confidence. Environ. Sci. Technol. 48, 2097–2098. https://doi.org/10.1021/es5002105

Tseng, H.H., Lee, W.W., Wei, M.C., Huang, B.S., Hsieh, M.C., Cheng, P.Y., 2012. Synthesis of TiO_2/SBA-15 photocatalyst for the azo dye decolorization through the polyol method. Chem. Eng. J. 210, 529–538. https://doi.org/10.1016/j.cej.2012.09.036

Van Grieken, R., Aguado, J., López-Muoz, M.J., Marugán, J., 2002. Synthesis of size-controlled silica-supported TiO_2 photocatalysts. J. Photochem. Photobiol. A Chem. 148, 315–322. https://doi.org/10.1016/S1010-6030(02)00058-8

Webler, A.D., Moreira, F.C., Dezotti, M.W.C., Mahler, C.F., Barbosa, I.D., Boaventura, R.A.R., Vilar, V.J.P., 2019. Development of an integrated treatment strategy for a leather tannery landfill leachate. Waste Manag. 89, 114–128. https://doi.org/10.1016/j.wasman.2019.03.066

Wei, J.Q., Chen, X.J., Wang, P.F., Han, Y.B., Xu, J.C., Hong, B., Jin, H.X., Jin, D.F., Peng, X.L., Li, J., Yang, Y.T., Ge, H.L., Wang, X.Q., 2018. High surface area TiO_2/SBA-15 nanocomposites : Synthesis, microstructure and adsorption-enhanced photocatalysis. Chem. Phys. J. 510, 47–53. https://doi.org/10.1016/j.chemphys.2018.05.012

Wilson, E.W., Castro, V., Chaves, R., Espinosa, M., Rodil, R., Quintana, J.B., Vieira, M.N., Santos, M.M., 2021. Using zebrafish embryo bioassays combined with high-resolution mass spectrometry screening to assess ecotoxicological water bodies

quality status: A case study in Panama rivers. Chemosphere 272, 129823. https://doi.org/10.1016/j.chemosphere.2021.129823

Xu, F., 2018. Review of analytical studies on TiO_2 nanoparticles and particle aggregation, coagulation, flocculation, sedimentation, stabilization. Chemosphere 212, 662–677. https://doi.org/10.1016/j.chemosphere.2018.08.108

Yang, J., Zhang, J., Zhu, L., Chen, S., Zhang, Y., Tang, Y., Zhu, Y., Li, Y., 2006. Synthesis of nano titania particles embedded in mesoporous SBA-15: Characterization and photocatalytic activity. J. Hazard. Mater. 137, 952–958. https://doi.org/10.1016/j.jhazmat.2006.03.017

Yuan, S., Wang, M., Liu, J., Guo, B., 2020. Recent advances of SBA-15-based composites as the heterogeneous catalysts in water decontamination: A mini-review. J. Environ. Manage. 254, 109787. https://doi.org/10.1016/j.jenvman.2019.109787

Zessel, K., Mohring, S., Hamscher, G., Kietzmann, M., Stahl, J., 2014. Biocompatibility and antibacterial activity of photolytic products of sulfonamides. Chemosphere 100, 167–174. https://doi.org/10.1016/j.chemosphere.2013.11.038

Zhao, D., Huo, Q., Feng, J., Chmelka, B.F., Stucky, G.D., 1998. Nonionic Triblock and Star Diblock Copolymer and Oligomeric Surfactant Syntheses of Highly Ordered, Hydrothermally Stable, Mesoporous Silica Structures. J. Am. Chem. Soc. 120, 6024–6036. https://doi.org/10.1021/ja974025i

Zhou, X-H., Huang, B-C, Zhou, T., Liu, Y-C., Shi, H-C, 2015. Aggregation behavior of engineered nanoparticles and theis impact on activated sludge in wastewater treatment. Chemosphere 119, 568–576. https://dx.doi.org/10.1016/j.chemosphere.2014.07.037

Declaration of interests

☒ The authors declare that they have no known competing financial interests or personal relationships that could have appeared to influence the work reported in this paper.

☐The authors declare the following financial interests/personal relationships which may be considered as potential competing interests:

CREDIT AUTHOR STATEMENTS

Bruna Castanheira: Conceptualization, methodology, validation, formal analysis, experimental investigation, data curation, writing – original draft; Larissa Otubo: Formal analysis, data curation, writing – original draft; Cristiano L. P. Oliveira: Formal analysis, data curation, writing – original draft; Rosa Montes: Formal analysis, data curation, writing – original draft; José Benito Quintana: Formal analysis, data curation, writing – original draft; Rosario Rodil: Formal analysis, data curation, writing – original draft; Sergio Brochsztain: Supervision, conceptualization, project administration, writing – original draft; Vítor J. P. Vilar: Supervision, conceptualization, project administration, writing – original draft, resources; Antonio Carlos S. C. Teixeira: Supervision, conceptualization, project administration, writing – original draft, resources, funding acquisition.

Supplementary Information

Functionalized mesoporous silicas SBA-15 for heterogeneous photocatalysis towards CECs removal from secondary urban wastewater

Bruna Castanheira[a], Larissa Otubo[b], Cristiano L. P. Oliveira[c], Rosa Montes[d], José Benito Quintana[d], Rosario Rodil[d], Sergio Brochsztain[e], Vítor J. P. Vilar[f,*], Antonio Carlos S. C. Teixeira[a,*]

[a]Research Group in Advanced Oxidation Processes (AdOx), Chemical Systems Engineering Center, Department of Chemical Engineering, Escola Politécnica, University of São Paulo, Av. Prof. Luciano Gualberto, tr. 3, 380, São Paulo, SP, Brazil

[b]Nuclear and Energy Research Institute (IPEN), Av. Prof. Lineu Prestes, 2242, 05508-000, São Paulo, SP, Brazil. [c]Institute of Physics, University of São Paulo, Rua do Matão 1371, 05508-090, São Paulo, SP, Brazil

[d]Department of Analytical Chemistry, Nutrition and Food Sciences, Institute of Research on Chemical and Biological Analysis (IAQBUS), Universidade de Santiago de Compostela, Constantino Candeira S/N, 15782 Santiago de Compostela, Spain.

[e]Federal University of ABC, Av. dos Estados, 5001, 09210-580, Santo André, SP, Brazil.

[f]Laboratory of Separation and Reaction Engineering-Laboratory of Catalysis and Materials (LSRE-LCM), Department of Chemical Engineering, Faculty of Engineering, University of Porto, Rua Dr. Roberto Frias, 4200-465 Porto, Portugal.

Corresponding authors: Antonio Carlos S. C. Teixeira (acscteix@usp.br)

Experimental details

Dosage of sulfadiazine (SDZ). The SDZ concentration was monitored by reversed-phase HPLC using a VWR Hitachi ELITE LaChrom fitted with a diode array detector (DAD) and a Merck LiChrosorb® RP-18 (5 μm) LiChroCART® 125–4 column at 25 °C. The mobile phase was an isocratic elution 80:20 (v/v) oxalic acid (0.014 M): acetonitrile with a mobile phase flow rate 0.7 mL min^{-1} during 5 min. Samples of 20 μL were injected and the DAD was set at λ of 265 nm. The retention time (*Rt*) was 3.4 min and the limits of quantification and detection were 0.18 and 0.05 mg L^{-1} of SDZ, respectively.

Dosage of SDZ at the μg/L level in UWW. The determination of SDZ levels in the UWW spiked with a low [SDZ] (40 μg L^{-1}) was made by solid-phase extraction (SPE) and Liquid Chromatography–Tandem Mass Spectrometry (LC–MS/MS). Briefly, 200 mL of sample were filtered (0.45 μm polyamide filters) and passed through a 500 mg Oasis HLB (Waters) cartridge, after washing and drying the cartridge, the analyte was recovered in 10 mL of MeOH. These methanolic extracts were injected in the LC-MS/MS (XEVO-TQD, Waters) system. The chromatographic separation was carried out in a Synergi 4μm fusion RP C18 100x2mm (Phenomenex) column using a gradient program with A: water (5mM ammonium acetate) and B: methanol (5mM ammonium acetate) as mobile phases. The gradient started at 2%B (0-1min) and increased to 100%B in 10 minutes, then remained at 100%B during 5 min, returned at initial conditions and keep this 2%B isocratic step for 5 min. The total run was 20 min. Two multiple-reaction monitoring (MRM) transitions were used as quantifier and qualifier respectively. These transitions were (precursor > fragment ion, m/z values): 251 > 92 and 251 > 156. The system operated in the electrospray positive (ESI +) ionization mode.

The quantification was performed by standard addition over the SPE methanolic extracts. The determination coefficient (R^2) was 0.9997 (5-5000 μg L^{-1}). The instrumental limit of quantification (IQL) was 5 μg L^{-1}.

Screening of other CECs in UWW. Urban wastewater (UWW) samples analysis was also performed with an Agilent 1290 Series LC (Agilent Technologies, Santa Clara, CA, USA) interfaced to an Agilent G6550B Series Quadrupole-Time of Flight (QTOF) mass spectrometer, equipped with a Dual Agilent Jet Stream Electrospray (Dual-AJS-ESI) ion source. The samples were analyzed in both positive and negative ionization modes. The chromatographic separation was performed in a ZORBAX Rapid Resolution HT 1.8 μm column at a mobile phase flow of 0.4 mL min^{-1}, and column temperature set to 35 °C. When working in ESI positive mode, the mobile phases consisted of Milli-Q water (eluent A) and methanol (eluent B), both containing 0.1% of formic acid. On the other hand, 5mM ammonium acetate was used as modifier in both (A) and (B) mobile phases instead of formic acid when working in ESI negative mode. Gradient was as follows: 0-2 min, 2% B; 22 min, 100% B; 26 min, 100% B; 26.10 min, 2% B; 30 min, 2% B. Nitrogen was used as nebulizing, drying and Collision-Induced Dissociation (CID) gas. The ESI source parameters were as follows: gas temperature 200 °C; drying gas 12 L min^{-1}; nebulizer 30 psig, capillary 2500 V and fragmentor 120 V. The instrument acquired MS spectra in centroid mode and operated at 2 GHz (extended-dynamic range), which provided a Full Width at Half Maximum (FWHM) resolution of ca. 9000-17,000. The scan range was 50−1000 m/z. A manufacturer reference solution was infused continuously during every run for a m/z-axis permanent recalibration according to manufacturer instructions. Tandem mass spectrometry (MS/MS) measurements were done in the "autoMSMS" (data-dependent) mode, thus, the system continuously selected the ions (*m/z*) with the highest abundance and

performed MS/MS experiments of these ions at three different collision energies (10, 20 and 40 V.). Precursor selection was limited to 2 ions per cycle and 3 MS/MS spectra (1 per collision energy). Three consecutive injections of the same sample were performed in the "iterative mode" where the system automatically excluded in each run the MS/MS precursor already fragmented in the previous injections of the same sample at the same retention time.

The software MassHunter Qualitative Analysis 10 (Agilent Technologies) was used for data treatment. Briefly, the algorithm "Find by autoMSMS" was used to generate a list of compounds which *m/z* and MS/MS spectra match to those MS/MS spectra from an accurate-mass library of 3320 chemicals that was built internally from different sources (Agilent ForTox, Agilent Water Screening, Agilent Metlin and Agilent Pesticides databases and direct injection of standards). Confirmation levels for each compound were stablished according to Schymanski *et al* [54] and only compounds with confirmation level 1 or 2 are reported. Tentatively identified compounds were then integrated from the single-MS extracted ion chromatogram (EIC) with a window set to reconstruction of the [M+H]+ or [M-H]- ion set to 50 ppm. The obtained areas were compared between the three analyzed conditions in order to obtain an estimation of the degradation yield.

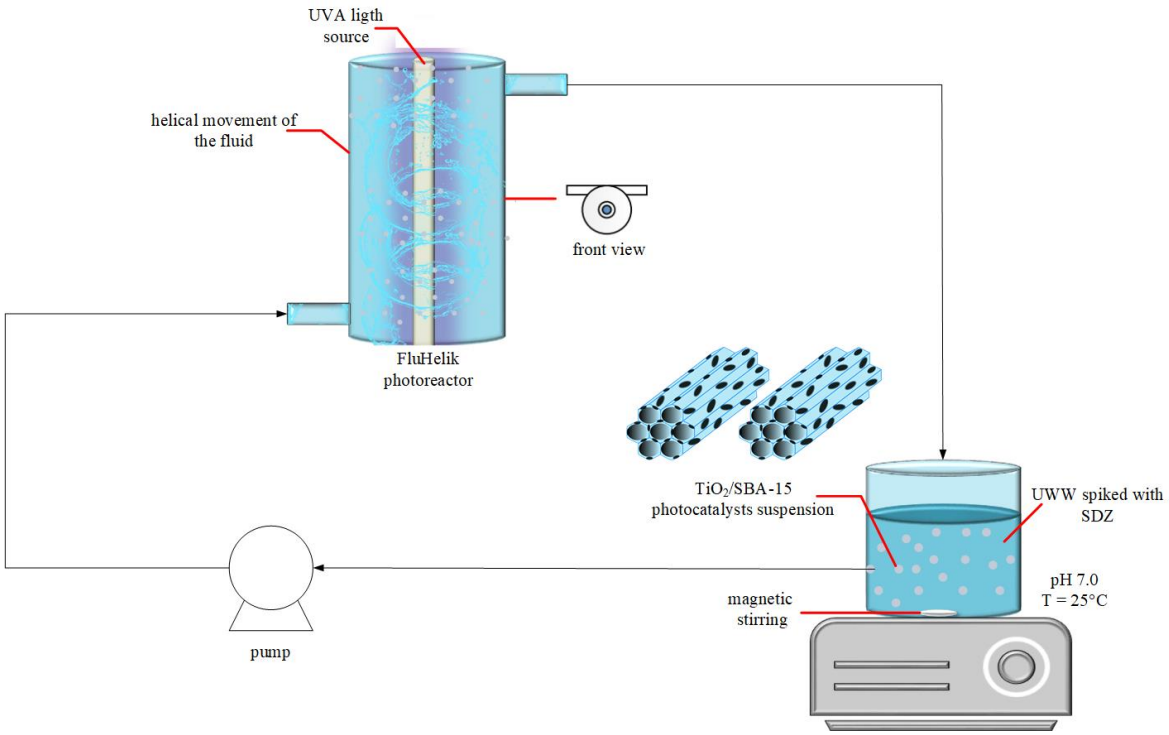

Figure S1. Schematics of the experimental set-up used for CECs oxidation.

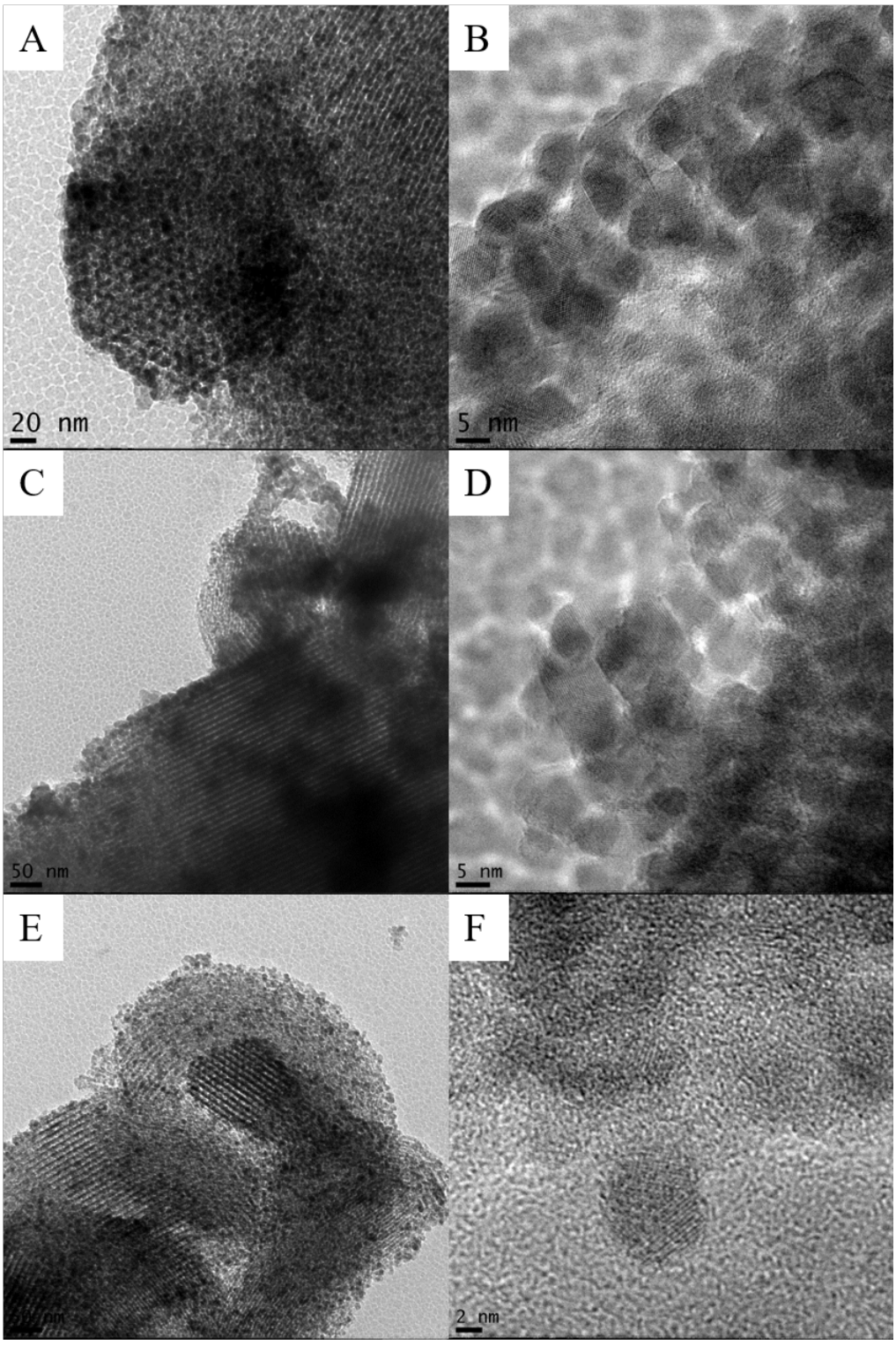

Figure S2. Additional HRTEM images of 10% TiO_2/SBA-15 (A, B), 20% TiO_2/SBA-15 (C, D) and 30% TiO_2/SBA-15 (E, F).

Table S1. Physicochemical characteristics of the secondary urban wastewater (UWW).

Parameters (units)	
Color	Pale/yellow
Odor	n.d.*
Turbidity (NTU)	0.34
pH	7.5
Temperature (°C)	25
Conductivity (mS cm^{-1})	2.4
Total dissolved carbon (mg L^{-1})	43.8
Dissolved inorganic carbon (mg L^{-1})	29.7
Dissolved organic carbon (mg L^{-1})	14.1
Chemical oxygen demand (mg L^{-1})	21.0
Absorbance at 254 nm (AU)	0.215
Transmittance at 254 nm (%)	61
Total suspended solids (mg L^{-1})	20.5
Volatile suspended solids (mg L^{-1})	16.0
Sulfate – SO_4^{2-} (mg L^{-1})	339
Nitrite – NO_2^- (mg L^{-1})	< 0.3
Nitrate – NO_3^- (mg L^{-1})	28
Total nitrogen (mg L^{-1})	52
Fluoride – F^- (mg L^{-1})	< 1
Chloride – Cl^- (mg L^{-1})	308
Phosphate – PO_4^{3-} (mg L^{-1})	< 4
Total phosphorous – P (mg L^{-1})	2.0

*n.d: not detected.

Table S2. Textural parameters of pristine SBA-15 and TiO_2/SBA-15 materials.

Sample	S_{BET} [a] ($m^2\ g^{-1}$)	V_p [b] ($cm^3\ g^{-1}$)	d [c] (nm)	a_0 [d] (nm)	wt [e] (nm)	L [f] (nm)
SBA-15	394	0.90	6.3	11.5	5.2	–
10% TiO_2/SBA-15	460	0.96	6.3	10.8	4.5	7.94
20% TiO_2/SBA-15	460	0.90	6.3	10.8	4.5	6.62
30% TiO_2/SBA-15	473	0.94	6.3	10.8	4.5	6.18

[a] Specific surface area (multipoint BET method). [b] Total pore volume (calculated at $P/P_0 = 0.97$). [c] Pore diameter (from BJH method, adsorption branch). [d] Lattice parameter determined from SAXS (Equation 1). [e] Wall thickness ($wt = a_0 - \text{pore diameter}$). [f] Average TiO_2 (anatase) crystallite size (Equation 2).

Table S3. Nomenclature, abbreviation, chemical formula, retention time (*Rt*) and application of the CECs in the UWW identified with LC-MS/MS analyzes.

Name	Abbreviation	Chemical Formula	*Rt* (min)	Name	Abbreviation	Chemical Formula	*Rt* (min)
Drugs for nervous system							
8-Chlorotheophylline	Ctp	$C_7H_7ClN_4O_2$	6.204	Memantine	MEM	$C_{12}H_{21}N$	8.835
Amantadine	AMD	$C_{10}H_{17}N$	4.925	Mirtazapine	MTZ	$C_{17}H_{19}N_3$	6.040
Amisulpride	AMI	$C_{17}H_{27}N_3O_4S$	5.433	Norcitalopram	N-CTA	$C_{19}H_{19}FN_2O$	9.309
Amitriptyline	AMT	$C_{20}H_{23}N$	11.294	O-Desmethylvenlafaxine (Desvenlafaxine)	O-DV	$C_{16}H_{25}NO_2$	5.815
Caffeine	Caf	$C_8H_{10}N_4O_2$	5.636	O-Desmethyltramadol	O-DT	$C_{15}H_{23}NO_2$	4.633
Carbamazepine	CBZ	$C_{15}H_{12}N_2O$	11.502	Riluzole	RZ	$C_8H_5F_3N_2OS$	11.622
Carbamazepine 10,11-epoxide	CBZ-E	$C_{15}H_{12}N_2O_2$	8.985	Sulpiride	SUL	$C_{15}H_{23}N_3O_4S$	3.200
Citalopram	CTA	$C_{20}H_{21}FN_2O$	9.250	Tapentadol	TAP	$C_{14}H_{23}NO$	6.830
Gabapentin	GABA	$C_9H_{17}NO_2$	3.329	Topiramate	TPM	$C_{12}H_{21}NO_8S$	9.205
Hydroxybupropion	HBUP	$C_{13}H_{18}ClNO_2$	6.526	Tramadol	TD	$C_{16}H_{25}NO_2$	6.349
Ketamine	KTM	$C_{13}H_{16}ClNO$	5.832	Trazodone	TZ	$C_{19}H_{22}ClN_5O$	8.003
Melperone	Me	$C_{16}H_{22}FNO$	7.269	Venlafaxine	VEN	$C_{17}H_{27}NO_2$	8.304
Drugs for cardiovascular system							
5-Hydroxypropafenone	5-OHPF	$C_{21}H_{27}NO_4$	9.593	Losartan	LOS	$C_{22}H_{23}ClN_6O$	13.279
Acebutolol	ACE	$C_{18}H_{28}N_2O_4$	6.914	Perindopril	PRD	$C_{19}H_{32}N_2O_5$	10.378
Bisoprolol	BIS	$C_{18}H_{31}NO_4$	8.543	Propranolol	PRN	$C_{16}H_{21}NO_2$	8.845
Celiprolol	CLP	$C_{20}H_{33}N_3O_4$	8.008	Sotalol	STL	$C_{12}H_{20}N_2O_3S$	2.396
Flecainide	FLE	$C_{17}H_{20}F_6N_2O_3$	9.398	Telmisartan	TEL	$C_{33}H_{30}N_4O_2$	13.042
Irbesartan	IST	$C_{25}H_{28}N_6O$	13.546				
Drugs for respiratory system							
Chlorpheniramine	CPMH	$C_{16}H_{19}ClN_2$	7.21	Fexofenadine	FEX	$C_{32}H_{39}NO_4$	11.709
Diphenhydramine	DPH	$C_{17}H_{21}NO$	9.146	Lidocaine (Diocaine)	LDC	$C_{14}H_{22}N_2O$	4.687
Doxylamine	DOX	$C_{17}H_{22}N_2O$	4.707				
Drugs for genito urinary system							

Alfuzosin	ALF	$C_{19}H_{27}N_5O_4$	8.228	Trospium	TSP	$C_{25}H_{30}NO_3$	8.437
Antiinfectives and antibacterials drugs							
Clarithromycin	CR	$C_{38}H_{69}NO_{13}$	11.091	Sulfapyridine	SPy	$C_{11}H_{11}N_3O_2S$	4.112
Sulfamethoxazole	SMX	$C_{10}H_{11}N_3O_3S$	6.269	Trimethoprim	TMP	$C_{14}H_{18}N_4O_3$	5.058
Dermatologicals drugs							
Climbazole	CLZ	$C_{15}H_{17}ClN_2O_2$	11.118	Fluconazole(II)	FLC	$C_{13}H_{12}F_2\ N_6O$	7.746
Drugs for musculo-skeletal							
Flufenamic acid	FA	$C_{14}H_{10}F_3NO_2$	15.783	Nimesulide	NIM	$C_{13}H_{12}N_2O_5S$	12.847
Niflumic acid	NIF	$C_{13}H_9F_3N_2O_2$	14.212				
Other pharmaceutical drugs							
Bicalutamide	BIC	$C_{18}H_{14}F_4N_2O_4S$	13.426	Levorphanol	LEV	$C_{17}H_{23}NO$	6.317
Diethyltoluamide	DEET	$C_{12}H_{17}NO$	12.259	Sitagliptin	SGN	$C_{16}H_{15}F_6N_5O$	6.869
Denatonium	DE	$C_{21}H_{29}N_2O$	9.267	Tiemonium	TI	$C_{18}H_{24}NO_2S$	6.554
Levofloxacin	LVX	$C_{18}H_{20}FN_3O_4$	5.640	Warfarin	WAR	$C_{19}H_{16}O_4$	13.440
Other substances							
Fipronil	FIP	$C_{12}H_4Cl_2F_6N_4OS$	15.769	Sucralose	SUC	$C_{12}H_{19}Cl_3O_8$	6.055
Nitrophenolate	NP	$C_6H_5NO_3$	6.144	Terbutryn	TB	$C_{10}H_{19}N_5S$	12.140
Ritalinic acid	RA	$C_{13}H_{17}NO_2$	5.993	Toluene-2-sulfonamide	TSN	$C_7H_9NO_2S$	5.886